

SINR-Aware Deep Reinforcement Learning for Distributed Dynamic Channel Allocation in Cognitive Interference Networks

Yaniv Cohen, Tomer Gafni, Ronen Greenberg, Kobi Cohen (*Senior Member, IEEE*)

Abstract—We consider the problem of dynamic channel allocation (DCA) in cognitive communication networks with the goal of maximizing a global signal-to-interference-plus-noise ratio (SINR) measure under a specified target quality of service (QoS)-SINR for each network. The shared bandwidth is partitioned into K channels with frequency separation. In contrast to the majority of existing studies that assume perfect orthogonality or a one-to-one user-channel allocation mapping, this paper focuses on real-world systems experiencing inter-carrier interference (ICI) and channel reuse by multiple large-scale networks. This realistic scenario significantly increases the problem dimension, rendering existing algorithms inefficient. We propose a novel multi-agent reinforcement learning (RL) framework for distributed DCA, named Channel Allocation RL To Overlapped Networks (CARLTON). The CARLTON framework is based on the Centralized Training with Decentralized Execution (CTDE) paradigm, utilizing the DeepMellow value-based RL algorithm. To ensure robust performance in the interference-laden environment we address, CARLTON employs a low-dimensional representation of observations, generating a QoS-type measure while maximizing a global SINR measure and ensuring the target QoS-SINR for each network. Our results demonstrate exceptional performance and robust generalization, showcasing superior efficiency compared to alternative state-of-the-art methods, while achieving a marginally diminished performance relative to a fully centralized approach.

Index Terms – Distributed channel allocation (DCA), wireless communications, cognitive interference networks, signal-to-interference-plus-noise ratio (SINR), deep reinforcement learning (DRL).

I. INTRODUCTION

The growing need for wireless communications, alongside the challenges posed by spectrum scarcity, has prompted the advancement of effective Dynamic Channel Allocation (DCA) schemes for emerging cognitive communication network technologies. Our focus is on DCA within large-scale networks, aiming to optimize the allocation of frequency channels among networks sharing the same frequency band. Unlike static channel allocation, where frequencies remain fixed, DCA adapts to changing network conditions by dynamically allocating channels based on factors such as interference

and signal strength, impacting user rates in the network. DCA enhances the efficiency and flexibility of wireless networks, ensuring efficient channel utilization and mitigating the impact of interference, leading to improved overall performance and quality of service (QoS). Recent studies on this topic, which involves learning the environment and channel allocation algorithms, have employed frameworks such as multi-armed bandits (MAB) [1]–[9], stable matching [10], [11], game theoretic optimization and congestion control [1], [8], [12]–[21], and, more recently, deep reinforcement learning (DRL) for multi-user scenarios [22]–[36]. The latter was initially explored in our earlier work (Naparstek and Cohen [22], [23]) within a multi-agent framework, following single-agent DRL research in [37], paving the way for a significant amount of subsequent research in the wireless communications community.

A. DRL Algorithms for DCA

DCA algorithms can be classified into two distinct branches: Centralized and distributed methods. Related studies within the centralized approach have utilized techniques such as graph vertex coloring, where adjacent vertices (representing users or local networks) are modeled with strong mutual interference, necessitating their allocation to different channels. Colors represent orthogonal channels, effectively coloring the graph. This paper addresses more challenging scenarios where interference exists between channels, and varies across the graph, for instance, decreasing with geographical distance, contrasting the binary interference assumption in graph coloring models. Additionally, centralized DRL methods have been recently proposed (see our recent work [36] and references therein). The limitation of the centralized approach lies in the communication overhead and computational complexity required for solving centralized DCA optimization. Consequently, in many applications, the preference is for distributed DCA, as it is widely considered more suitable for various wireless communication scenarios due to the intricate nature of the problem.

In this paper, we focus on DRL methodology to address the distributed DCA problem. In recent years, the notable achievements of DRL in attaining strong performance surpassing human capabilities across various game domains have captured the attention of researchers from various disciplines. Prominent examples include its successes in games such as Atari [38], [39], Go [40], and even in complicated game such as StarCraft II [41]. This success has motivated researchers

Corresponding author: K. Cohen, yakovsec@bgu.ac.il. K. Cohen and T. Gafni are with the School of Electrical and Computer Engineering, Ben-Gurion University of the Negev, Beer Sheva 8410501 Israel. Y. Cohen and R. Greenberg are with Elbit Radio Ltd., Israel.

This work was supported by the Israel Ministry of Economy under the Magnet consortium program.

This work has been submitted to the IEEE for possible publication. Copyright may be transferred without notice, after which this version may no longer be accessible.

to explore the development of DRL in diverse fields such as robotics, biology, chemistry, finance [42], as well as wireless communications [22]–[31], [34], [43]. This approach is particularly promising in the topic of DCA, where the collection of data becomes inefficient due to the high dimensionality of the state space resulting from the numerous uncertainties inherent in the environment. Particularly, recent study [33] proposed a model-free Multi-Agent Reinforcement Learning (MARL) independent Q-learning (IQL) table approach to solve the distributed DCA problem over orthogonal channels. While this work demonstrates the potential of a simple RL technique for addressing the DCA challenge, it is limited to small-scale systems due to the high dimensionality of the state space in the DCA problem. To overcome this limitation, the state space was reduced and strongly quantized in the conducted study. Additionally, the IQL technique, both in a general context and specifically in the domain of radio systems, imposes constraints on system scalability. This arises from the inherent characteristic wherein each agent acquires an independent policy, which is greatly dependent on the policies formulated by the other participating agents. Furthermore, recently in [35], the authors employed the Double Deep Q-network (DDQN) [44] as the RL optimization mechanism to solve DCA in multi-agent systems. This utilization of the DDQN facilitates the exploration of more effective strategies. The transition from a tabular approach to neural networks (NN) diminishes the dependence on quantization techniques employed in previous research, leading to an improved generalization of the problem. In [32], an attention-based Graph Neural Network (GNN) architecture known as GA-Net, was introduced. The study addressed DCA in 6G sub-networks using a centralized training approach and a decentralized execution paradigm. The authors assumed channel orthogonality and employed a modified Soft-Actor-Critic (SAC) algorithm as the optimization technique for MARL system. By combining the hard attention layer with the Graph Attention Network (GAT), the proposed algorithm demonstrated improved performance by effectively extracting relevant features that capture the relationships between different sub-networks compared to other techniques examined in [32]. Motivated by the recent success of DRL in DCA, our paper takes on a challenge that has not yet been effectively addressed. Specifically, here we focus on developing a DRL framework for distributed DCA among large-scale cognitive interference networks. This framework accommodates channel reuse, continuous interference over the network graph, all without assuming complete orthogonality due to ICI.

B. Main Results

Multi-agent DRL for DCA has garnered significant attention in recent years, spurred by our earlier work [22], [23]. In contrast to related recent studies that predominantly centered around relatively small-scale networks, often addressing singular sensor-controller low-power links within enclosed environments (e.g., robotic systems), the present study introduces a distributed DCA algorithm tailored for large-scale network configurations. This algorithm places paramount importance on attaining elevated channel quality (CQ) while concurrently

minimizing convergence time in outdoor scenarios. Additionally, in contradistinction to existing studies that assumed orthogonal channel conditions, our approach confronts the intricate complications arising from ICI across channels, where orthogonality is not preserved. It underscores the need for minimal spectrum mobility, an imperative requirement for distributed networks supporting a multitude of users. The realistic challenging scenario considered in this paper significantly increases the search space, rendering existing algorithms inefficient.

To tackle this problem, we propose a novel MARL framework for distributed DCA, named Channel Allocation RL To Overlapped Networks (CARLTON). The CARLTON framework is based on the Centralized Training with Decentralized Execution (CTDE) paradigm, utilizing the DeepMellow value-based RL algorithm [45]. DeepMellow’s design mitigates the necessity for a target network in comparison to conventional DQN algorithms. To ensure robust performance in the interference-laden environment we address, CARLTON quantizes observations to generate a QoS-type measure while maximizing a global SINR measure and guaranteeing the target QoS-SINR for each network. CARLTON incorporates a novel reward framework that trades off personal rewards with social rewards, encouraging cooperative behavior among distinct networks incapable of information exchange. Moreover, we introduce a preprocessing mechanism designed to enhance the algorithm’s adaptability to diverse network sizes. Within our specific problem domain, each network receives an exclusive sensed vector, representing only a fraction of the comprehensive state information inherent in the MARL environment. Consequently, the problem discussed herein inherently falls within the domain of Partially Observable Markov Decision Process (POMDP) problems.

The proposed CARLTON algorithm has demonstrated exceptional performance and robust generalization capabilities, outperforming various alternative methods. This includes surpassing the common random agent (RA) benchmark [20] and, notably, outperforming the state-of-the-art method for our model, the well-known Jamming Avoidance Response (JAR) algorithm [46]. CARLTON demonstrated a remarkable approximate margin of superiority of 45% over the RA benchmark and 20% over the JAR algorithm, respectively. Furthermore, it exhibits only a slight discrepancy of approximately 2.5% in performance compared to a centralized approach computed by graph coloring. This level of effectiveness positions CARLTON as an outstanding algorithm for efficiently managing DCA among distributed cognitive networks in complex interference environments.

II. SYSTEM MODEL AND PROBLEM FORMULATION

A. Description of the System

We consider a system comprising N wireless networks represented by the set $\mathcal{N} = \{\mathcal{N}^1, \dots, \mathcal{N}^N\}$. Each network (say \mathcal{N}^n) accommodates M^n users, with $M^n \in \{1, 2, \dots, M_{max}\}$, and M_{max} denoting the maximum number of users among all networks. A total bandwidth (TB) is equally divided into K equal-sized overlapping channels with bandwidth B denoted

by the set $\mathcal{K} = \{1, 2, \dots, K\}$ such that each network can operate on a single channel at each time slot. Orthogonality is not maintained across carriers, resulting in ICI between channels. In this context, we index the channels based on their serial numbers in \mathcal{K} , as depicted in Figure 1.

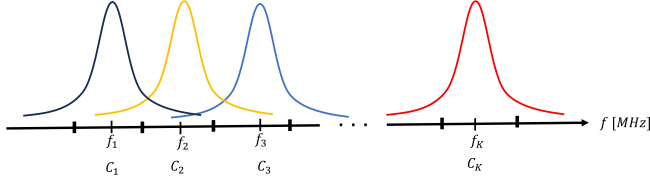


Fig. 1: An illustration of the non-orthogonal channel partition. Channel i , denoted by C_i in the figure, refers to the carrier frequency f_i .

To model the interference between networks, we employ the well-established Egli model [47]. The Egli model, developed for UHF and VHF outdoor signals, is commonly used for modeling real-world radio frequency propagation. Based on the model, the SINR of each user at each available channel is computed. The SINR accounts for the interference from the other networks in the environment, and the additive thermal noise at the receiver. In what follows, to describe the computation, we use the indexing notations

$$(\cdot)_{m,j,k}^{l,n} \quad (1)$$

to represent a parameter regarding a pair of users, denoted as user $m \in \mathcal{N}^l$ and user $j \in \mathcal{N}^n$. The SINR is computed with respect to channel k . When the parameter pertains to a single user, irrespective of the presence of a second user, we specify only a single user. Specifically, the SINR of users within network $\mathcal{N}^n \in \mathcal{N}$ on channel $k \in \mathcal{K}$ is computed as follows. Consider users $i, j \in \mathcal{N}^n$, where user i transmits a message to user j , operating on channel $k \in \mathcal{K}$. The received SINR at the receiver of user j is given by:

$$\text{SINR}_{i,j,k}^{n,n} = \frac{\text{PR}_{i,j,k}^{n,n}}{I_T + I_{j,k}^n}, \quad (2)$$

where $\text{PR}_{i,j,k}^{n,n}$ is the signal power at the receiver of user $j \in \mathcal{N}^n$ transmitted by user $i \in \mathcal{N}^n$ on channel k , I_T is the additive thermal noise power, and $I_{j,k}^n$ is the interference power at the receiver of user $j \in \mathcal{N}^n$ on channel k . This interference is attributed to all other networks $\mathcal{N} \setminus \mathcal{N}^n$ transmitting on any possible channel, with ICI modeled by the Egli model, as computed later. Interference between users within the same network is avoided by the Medium Access Control (MAC) scheduler mechanism. The computation of the received power is given by:

$$\text{PR}_{i,j,k}^{n,n} = \text{PT}_{j,k}^n - \text{PL}_{i,j,k}^{n,n}, \quad (3)$$

where $\text{PT}_{j,k}^n$ is the transmitter power of user $j \in \mathcal{N}^n$ on channel k (possibly broadcasted signal irrespective of user $j \in \mathcal{N}^n$) in dBW, and $\text{PL}_{i,j,k}^{n,n}$ is the path loss between user $j \in \mathcal{N}^n$ and user $i \in \mathcal{N}^n$ on channel k , which obeys the Egli

model and is given by:

$$\begin{aligned} \text{PL}_{i,j,k}^{n,n} &= 40 \log_{10}(d_{i,j}^{n,n}) \\ &\quad - 20 \log_{10}\left(\frac{40}{f_k}\right) - 20 \log_{10}(H_{T_j}^n H_{R_i}^n) \\ &\quad - 10 \log_{10}(G_{T_i}^n G_{R_j}^n) \text{ [dB]}, \end{aligned} \quad (4)$$

where $d_{i,j}^{n,n}$ is the euclidean distance between users $j \in \mathcal{N}^n$ and $i \in \mathcal{N}^n$ in [meters], f_k is the carrier frequency of channel k in [MHz], $H_{T_j}^n$ and $H_{R_i}^n$ are the heights of the transmit and receive antennas of users $j \in \mathcal{N}^n$ and $i \in \mathcal{N}^n$ in [meters], respectively, and $G_{T_i}^n$ and $G_{R_j}^n$ are the absolute gain of the transmitter and receiver antennas of users $j \in \mathcal{N}^n$ and $i \in \mathcal{N}^n$, respectively.

The interference power from other networks $\mathcal{N} \setminus \mathcal{N}^n$ at the receiver of user $j \in \mathcal{N}^n$ on channel k is given by:

$$I_{j,k}^n = \sum_{l \in \{1, \dots, n-1, n+1, \dots, N\}} \Phi_{j,k}^{n,l} \quad (5)$$

where

$$\Phi_{j,k}^{n,l} \triangleq \sum_{m \in \{1, \dots, M^l\}} \phi_{j,m,k}^{n,l},$$

where $\phi_{j,m,k}^{n,l}$ is the interference power from user $m \in \mathcal{N}^l$, given by:

$$\phi_{j,m,k}^{n,l} = \text{PR}_{j,m,k}^{n,l} - T(k, \tilde{k}) \quad (6)$$

where \tilde{k} is the channel used by network \mathcal{N}^l , and $T(k, \tilde{k})$ is the attenuation at the channel of interest k with respect to channel \tilde{k} . The attenuation used in the simulations in this paper is given in Table I [48].

Spectral Distance $ k - \tilde{k} $	Attenuation (dBm)
0	0
1	20
2	40
3	50
4	60
≥ 5 and $ f_k - f_{\tilde{k}} /f_k \leq 0.05$	95
else	110

TABLE I: Attenuation with respect to spectral distance, where f_k and $f_{\tilde{k}}$ represent the frequencies of channels k and \tilde{k} , respectively.

The thermal noise I_T at the receiver is calculated as follow:

$$\begin{aligned} I_T &= k_B \cdot \text{Temp} \cdot B \cdot \text{NF} \text{ [W]} = \\ &10 \log_{10}(k_B \cdot \text{Temp} \cdot B) + 10 \log_{10}(\text{NF}) + 30 \text{ [dBm]}, \end{aligned} \quad (7)$$

where k_B , Temp, B , and NF stands for Boltzmann constant, temperature, bandwidth, and noise figure. For instance, at room temperature, bandwidth of 2MHz , and $10 \log_{10}(\text{NF}) = 6$, we have $I_T = -104.9 \text{ [dBm]}$.

B. Illustration of the System Environment in Real-World Simulations

To elaborate on the system model and its significant relevance in dynamic spectrum access systems, we present a comprehensive depiction of the system environment through real-world simulation settings that inspire this research. In each

simulation instance, a specific number of networks, denoted as N , is randomly chosen. For each network, the number of users is randomly assigned, following a uniform distribution (ranging from 2 to 22 users in our simulations). The spatial distribution of users within each network is determined by a multi-variate Gaussian distribution. The expectation vector is defined by a 2D center point, and the covariance is represented by a diagonal matrix with entries $[50^2, 50^2]$ $[m^2]$. It is noteworthy that our current investigation primarily addresses a 2D spatial problem, but the methodology can be readily extended to encompass 3D dimensions. The center point for each network is determined using the procedure outlined in Algorithm 1.

Algorithm 1 - Set Networks Center Points Locations

Input: N ▷ Number of networks
Output: μ ▷ Dictionary of all center points, $\mu \in \mathbb{R}^{2 \times N}$
 1: $\mu \leftarrow \{\}$ ▷ Define empty dictionary
 2: **for** $i \in \{1, \dots, N\}$ **do**
 3: **if** $i == 0$ **then**
 4: $\mu_x^0 \leftarrow u_x$ s.t. $U_x \sim U[-u_1 N, u_1 N]$
 5: $\mu_y^0 \leftarrow u_y$ s.t. $U_y \sim U[-u_1 N, u_1 N]$
 6: **else**
 7: $\mu^c =$ choose random center point from μ
 8: $r \leftarrow$ sample from $U[x_1, x_2]$
 9: $\theta \leftarrow$ sample from $U[0, 2\pi]$
 10: $\mu_x^i \leftarrow \mu_x^c + r \cos(\theta)$
 11: $\mu_y^i \leftarrow \mu_y^c + r \sin(\theta)$
 $\mu[i] \leftarrow (\mu_x^i, \mu_y^i)$

In our simulation environment, we incorporate the concept that each network includes a specific user designated as the *network manager*, aligning with the common practice in 5G technology where centralized units oversee local networks. The network manager is selected as the user within the network whose total Euclidean distance from all other users in the same network is minimized. This selection is based on the user's ability to maintain the shortest average distance to all other users within the given network. The role of the network manager is pivotal, taking on the responsibility of gathering information from other users within the network and disseminating decisions as feedback. This feedback mechanism fosters effective communication and coordination among users, allowing the network manager to serve as a central point for control and information exchange within its respective network, using a dedicated control channel. By fulfilling this crucial function, the network manager significantly contributes to optimizing the overall efficiency of the network's operations. Figure 2 illustrates a representative scenario, featuring a possible configuration of networks, each accompanied by its designated network manager.

C. The Objective

Let $c^n \in \{1, \dots, K\}$ represent the operating channel of network \mathcal{N}^n , and SINR_{j,c^n}^n be the average SINR of user $j \in \mathcal{N}^n$, computed in consideration of all messages received from

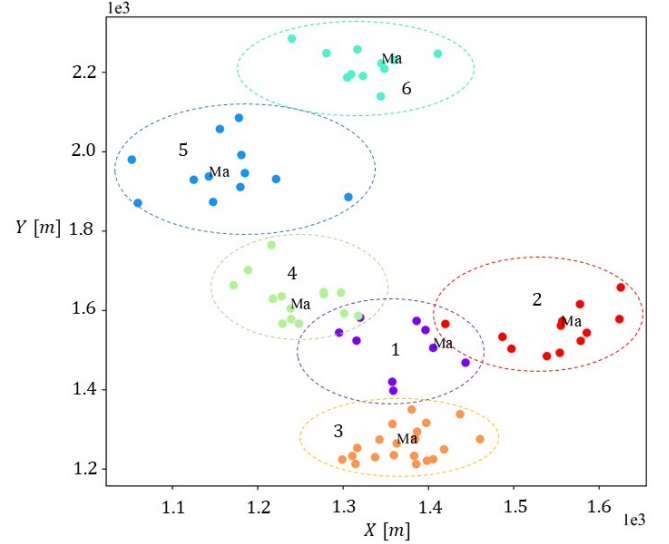


Fig. 2: An illustration of the simulation environment involving six networks. Each color corresponds to a distinct network, distinguished by a unique serial number. The symbol 'Ma' denotes the network manager present at each respective network.

the other $M^n - 1$ users in network \mathcal{N}^n . Then, SINR_{j,c^n}^n is given by:

$$\text{SINR}_{j,c^n}^n = \frac{1}{M^n - 1} \sum_{\substack{i=1 \\ i \neq j}}^{M^n} \text{SINR}_{j,i,c^n}^n. \quad (8)$$

Then, the average SINR of network \mathcal{N}^n , denoted by $\overline{\text{SINR}}_{c^n}^n$, is given by:

$$\overline{\text{SINR}}_{c^n}^n = \frac{1}{M^n} \sum_{j=1}^{M^n} \text{SINR}_{j,c^n}^n. \quad (9)$$

The objective is to maximize the average $\overline{\text{SINR}}_{c^n}^n$ across all participating networks, subject to the constraint that the $\overline{\text{SINR}}_{c^n}^n$ for each network exceeds the target QoS-SINR required for high-quality communication, defined by SINR^* :

$$\begin{aligned} & \max_{\{c^n\}^N} \frac{1}{N} \sum_{n=1}^N \overline{\text{SINR}}_{c^n}^n \\ & \text{subject to } \overline{\text{SINR}}_{c^n}^n \geq \text{SINR}^* \quad \forall n \in \mathcal{N}, \end{aligned} \quad (10)$$

Two crucial requirements for the algorithm are identified. Firstly, the algorithm must exhibit a short convergence time to swiftly adapt to the dynamic nature of the spectrum environment, ensuring timely and efficient allocation of available resources. Secondly, a distributed implementation is imperative to promote scalability, enhance flexibility, and reduce the computational burden on individual nodes, fostering a more resilient and adaptable system architecture.

III. THE CHANNEL ALLOCATION RL TO OVERLAPPED NETWORKS (CARLTON) ALGORITHM

In this section, we introduce the CARLTON algorithm designed to address the objective. We formulate the DCA problem as a MARL framework, where each network manager acts

as an autonomous agent within the global framework. Consistent with standard Reinforcement Learning (RL) paradigms, the well-defined environment comprises observation, action, and reward components. Following the system model outlined in Section II, the CARLTON framework enables network managers (agents) to iteratively learn and adapt their channel allocation strategies, aiming for improved channel quality and reduced spectrum mobility until the system converges to a desirable solution. We commence by addressing and defining the mentioned requirements in detail.

A. Observation Space

The observation space encompasses a fusion of SINR measurements from all users within the network. Before the network manager makes a decision, each user transmits its individual SINR measurements for all available channels via a dedicated control channel to the network manager. This vector of SINR measurements has a dimension of \mathbb{R}^K (SINR value for each channel).

The network manager, after conducting SINR sensing for all channels, receives unique SINR measurement vectors from all users in the network. These individual vectors are then concatenated to form an SINR matrix with dimensions $\mathbb{R}^{M^n \times K}$, where M^n corresponds to the total number of users in network \mathcal{N}^n . The entry $\text{SINR}_{j,k}^n$ at row j and column k of the matrix, where $j = 1, \dots, M^n$ and $k = 1, \dots, K$, represents the SINR measurement for user j on channel k . Additionally, we define a binary matrix BSINR^n with dimensions $M^n \times K$, where each entry is set to either 0 or 1, indicating whether the corresponding $\text{SINR}_{j,k}^n$ value is below or above the target QoS-SINR threshold, respectively:

$$\text{BSINR}_{j,k}^n = \mathbb{1}(\text{SINR}_{j,k}^n > \text{SINR}^*), \quad (11)$$

where $\mathbb{1}$ is the indicator function, equals 1 if $\text{SINR}_{j,k}^n > \text{SINR}^*$, or equals zero otherwise.

Next, the network manager performs an averaging operation on the BSINR^n matrix along the user axis to mitigate the influence of the number of users in the network. The k th entry of the vector for channel k is given by:

$$\text{QV}_k^n = \frac{1}{M^n} \sum_{j=1}^{M^n} \text{BSINR}_{j,k}^n. \quad (12)$$

This averaging process results in a vector representing the average number of users experiencing sufficient communication quality. We will refer to this vector as the Quality Vector ($\text{QV}^n \in \mathbb{R}^K$), which serves as a key observation in the simulations.

B. Action Space

The action space encompasses the set of allowable actions available to the agent at each decision point. In the current context, the action space includes all possible frequency channels and is represented by \mathcal{K} . Thus, at each time step, the action of network \mathcal{N}^n is defined as $a^n(t) \in \mathcal{K}$.

C. Reward

The agents are tasked with solving a combinatorial problem, namely, establishing a one-to-one mapping between each network and a channel. The objective is to reach a state where, either upon convergence (where each network remains connected to the same chosen channel until the completion of the scenario) or at the end of the scenario, the total mean quality of the selected channels across all networks is maximized, as detailed in Section II-C.

To pursue this objective, we embrace a two-part reward value, consisting of two distinct components. The first element relates to the personal reward, denoted by r_p . Its magnitude is influenced by the $\text{QV}^n(t)$ value associated with the channel quality ranking selected by the agent pre-selection cycle of all other networks at time step t . Essentially, r_p reflects a greedy mechanism aimed at selecting high-quality channels. Additionally, the personal reward experiences positive growth if the action remains unchanged. The reward computation is elucidated in Algorithm 2.

Algorithm 2 CARLTON's Personal Reward, r_p

Input: $\text{QV}^n(t), a^n(t), a^n(t-1)$ $\triangleright a^n(t)$ is the chosen channel at time t

Output: r_p

- 1: $v \leftarrow \text{QV}_{a^n(t)}^n(t)$ \triangleright Extract the $\text{QV}^n(t)$ value of the chosen channel
- 2: **if** $v \geq \zeta$ **then**
- 3: $r_p \leftarrow r_{desired}$
- 4: **else**
- 5: $\text{SQV}^n \leftarrow \text{sort}(\text{QV}^n(t))$
- 6: $i \leftarrow 0$
- 7: **while** $i \leq K \cap v \geq \text{SQV}_i^n$ **do**
- 8: $i \leftarrow i + 1$
- 8: $r_p \leftarrow 2(\frac{i}{K} - 0.5)$
- 9: **if** $a^n(t) == a^n(t-1)$ **then**
- 10: $r_p \leftarrow c_1 \cdot r_p$ $\triangleright c_1$ is constant > 1

The second component of the reward mechanism is designated as the *social welfare reward*, denoted by r_{sw} . This reward takes into consideration the implications of a network's actions on the individual rewards of its neighboring networks during the interval between two consecutive decision-making instances. Specifically, a network is categorized as a neighboring network if the Euclidean Distance (ED) between their network center points is less than a predetermined threshold, represented as Γ meters. In essence, r_{sw} captures the collective welfare and interdependence among the networks, accounting for the influence exerted by the behavior of each network on the rewards of others over successive iterations. The social welfare reward is calculated as the arithmetic mean of the personal rewards of all neighboring networks. The pseudo-code for the social welfare reward is outlined in Algorithm 3.

Finally, the total reward is a linear combination of the two reward terms:

$$r = \rho r_p + (1 - \rho) r_{sw}, \quad (13)$$

Algorithm 3 CARLTON's Social Welfare Reward, r_{sw}

Input: R_p, i, μ, Γ ▷ List of
 all r_p of other networks between two consecutive decision
 points, the index of the network of interest, dictionary of
 all center points, and constant value

Output: r_{sw}

- 1: $n \leftarrow 0$
- 2: $r_{sw} \leftarrow 0$
- 3: **for** $j \in \{1, \dots, N\}$ **do**
- 4: **if** $\text{ED}(\mu[j], \mu[i]) \leq \Gamma \cap j \neq i$ **then**
- 5: $n \leftarrow n + 1$
- 6: $r_{sw} \leftarrow \frac{1}{n} ((n-1)r_{sw} + r_p^j)$

where $\rho \in [0, 1]$ is a design parameter.

D. Training Procedure

CARLTON adheres to the multi-agent paradigm known as Centralized Training with Decentralized Execution (CTDE). At the beginning of each episode, each individual agent, denoted as the network manager, is assigned an exclusive serial number. This serial number determines the timing of its actions, effectively simulating a delay time characteristic of real-world scenarios. This technique is strategically employed to circumvent the potential collision of decisions among different networks and to mitigate the overall dynamic complexity of the scenario. To ensure a consistent and balanced decision-making process, the scenario horizon is explicitly defined as T times the total number of participating networks within the given scenario. Consequently, this arrangement allows each network to possess precisely T decision points per scenario, guaranteeing equitable opportunities for each participant to influence the outcome of the scenario.

The resource allocation concerning channel frequency selection during the training phase conducted by each agent adheres to the following prescribed methodology. In particular, with a probability denoted by ϵ_b , the agents draw samples from the distribution in (14), originally introduced in the Exp3 algorithm for the non-stochastic multi-armed bandit problem [49]. Otherwise, the agents follow a greedy policy:

$$\Pr(a^n(t) = k | s^n(t)) = \frac{(1 - \alpha)e^{\beta Q(s^n(t), k; \theta)}}{\sum_{a' \in \{1, \dots, K\}} e^{\beta Q(s^n(t), a'; \theta)}} + \frac{\alpha}{K} \quad \forall k \in \mathcal{K}. \quad (14)$$

Here, $s^n(t)$ stands for the state at time step t of network \mathcal{N}^n , $Q(s^n(t), k; \theta)$ stands for the estimated action value by the NN with weights θ , which its architecture described below, and α and β are constants. Additionally, during the training period comprising B episodes, we annealed ϵ_b from 0.5 to 0.01 after each of the first $B/2$ episodes, and then maintained it at a steady value for the remaining half, i.e., the latter $B/2$ episodes.

Furthermore, an additional step involves the application of an action-masking technique over the $Q(s^n(t), a^n(t))$ values, which is based on the QV^n values on each channel k . For any channel in QV^n with a value of 0, the probability of selecting this channel is masked to 0, while in the event of $\text{QV}^n = \vec{0}$,

no action selection is performed, and the previous action is preserved. This technique serves the purpose of preventing collisions among different networks and is mathematically executed as follows:

$$Q(s^n(t), k; \theta) = \begin{cases} -\infty, & \text{if } \text{QV}_k^n = 0, \\ Q(s^n(t), k; \theta), & \text{otherwise.} \end{cases} \quad (15)$$

Next, as is inherent in DRL value-based algorithms, our principal objective is to find an estimating function, denoted as f_θ , which approximates the action value $Q(s^n(t), a^n(t); \theta)$. This function adeptly maps any given set of state and action (s, a) to a real number within the domain of \mathbb{R} . The optimization of f_θ is commonly achieved through gradient descent algorithms over a differentiable loss function. In this context, we employ the Huber loss to compute our loss value. The Huber loss function is given by:

$$L_\delta(e) = \begin{cases} \frac{1}{2}e^2, & \text{if } |e| \leq \delta, \\ \delta \cdot (|e| - \frac{1}{2}\delta), & \text{otherwise,} \end{cases} \quad (16)$$

where $e^n = (r^n(t) + \gamma \text{mm}_\omega Q(s^n(t+1), a'; \theta) - Q(s^n(t), a^n(t); \theta))$, and mm_ω is a smooth maximum operator named Mellowmax operator with a temperature parameter ω [50]. Generally, e is the error between the target and predicted values, and δ is a discrimination hyper-parameter threshold. Subsequently, with the aid of these estimated action values, the learn policy can be derived. To enable this process, we formally define the input state as follows:

$$s^n(t) = \text{concatenate}(\text{CBR}, \text{QV}^n(t)). \quad (17)$$

Here, the term CBR represents the Channel Binary Representation, refers to the channel that the network utilizes before executing the action. In other words, it is a binary representation of the preceding action if the action was fulfilled. The term $\text{QV}^n(t)$ stands for the QV^n at time step t .

The NN architecture of CARLTON consists of three dense layers with skip connections. The hidden layer uses the Leaky-ReLU activation function with a slope of 0.2, while the output layer employs the identity activation function. Furthermore, to initialize the weights of the NN, the Glorot-Uniform method, as introduced in the work by Glorot and Bengio [51], is applied, and the biases are initialized to zero.

The training procedure unfolds across B scenarios as follows: First, within each main training loop, we uniformly sample the number of participating networks. Subsequently, we generate a scenario following the rules outlined in Section II-B. For each network, we then randomly assign a network number $n \in 1, \dots, N$ to define \mathcal{N}^n and allocate a unique replay memory (\mathcal{D}^n). Next, we iterate over T time steps for each scenario, where at each step we execute actions for each network sequentially, corresponding to their assigned network number. Then, we store the relevant information in the respective unique replay buffer. Upon scenario completion, we transfer data from each \mathcal{D}^n into a global replay memory (GRM). Subsequently, we uniformly sample from the GRM and train the NN by minimizing (16) N_E times.

The training procedure is illustrated in Algorithm 4, providing a comprehensive outline of the steps involved. For a clear

overview of the hyperparameters utilized during the training process, please refer to Table II.

Algorithm 4 CARLTON's Training Procedure

Input: All hyperparameters in Table II

Input: Initialize NN weights, θ_0

Output: Trained mechanism for distributed DCA, θ^*

- 1: Create Global Replay memory (GRM) of size S_z
 - 2: **for** $i \in \{1, \dots, B\}$ **do**
 - 3: Uniformly sample random number of networks
 - 4: Set a random scenario with N networks (Section II-B)
 - 5: Randomly match unique network numbers
 - 6: Create Local Replay Memory (\mathcal{D}^n) for each network
 - 7: Randomly initialize each network to some channel
 - 8: **for** $t \in \{1, \dots, T\}$ **do**
 - 9: **for** $n \in \{1, \dots, N\}$ **do**
 - 10: obtain $QV^n(t)$
 - 11: $s^n(t) \leftarrow \text{concatenate}(\text{BCR}, QV^n(t))$
 - 12: Store $(s^n(t-1), a^n(t-1), r^n(t), s^n(t))$ in \mathcal{D}^n
 - 13: Select $a^n(t)$ for \mathcal{N}^n based on $f_{\theta_{i-1}}$
 - 14: Execute $a^n(t)$ and observe r_p^n
 - 15: Store all data in local \mathcal{D}^n in GRM $\forall n \in \{1, \dots, N\}$
 - 16: **for** $\{1, \dots, N_E\}$ **do**
 - 17: Uniformly sample a mini-batch of size b_z ,
 - 18: $(s(t), a(t), r(t), s(t+1)) \sim \text{GRM}$
 - 19: Train the NN by minimizing (16) and obtain θ_i
-

IV. EXPERIMENTS AND DISCUSSION

In this section, we present comprehensive experimental results to illustrate the efficiency of the proposed CARLTON algorithm in a real-world simulation environment, as described in Section II. We commence by analyzing specific features in the training procedure of CARLTON in Subsection IV-A. Subsequently, we provide a performance comparison with state-of-the-art methods in Subsection IV-B.

A. CARLTON's Training Results

CARLTON undergoes two distinct training scenarios, one involving the action masking approach, as referenced in (15), and the other without it. As expected, the incorporation of masking during action selection results in higher accumulated rewards during the initial phases of training (Episodes ≤ 400). This improvement stems from the reduction of unnecessary exploration, as illustrated in Figure 3. However, as training progresses and convergence is achieved (Episodes ≥ 500), both techniques yield comparable results. It is important to note that both approaches remain applicable when the messages exchanged between network users and the network manager are transmitted through a control channel, which is assigned and freed for communication at any given time.

On the other hand, in situations where no dedicated control channel is available, the utilization of masking becomes essential to ensure the existence of a functional communication link between the users and the network manager. Thus, it guarantees that there is at least some form of connection

Parameter	Value
Number of channels, K	10
Channels frequencies carriers, $\{f_1, \dots, f_k\}$ [MHz]	$\{208, \dots, 226 f_{k+1} - f_k = 2MHz\}$
Antennas gains, G_R, G_T	1
Antennas heights (H_R, H_T) [m]	1
Transmit power, PT [dBW]	2
Range of initial center point, u_1 [m]	400
Radius range, x_1, x_2 [m]	50, 500
The set of possible users per network, \mathcal{M}	$\{1, \dots, 15\}$
SINR threshold, SINR* [dBm]	4
Desired reward, $r_{desired}$	4
Constant, c_1	1.1
A desired threshold, ζ	0.9
Euclidean distance threshold which defines a network as a neighbor Γ [m]	500
Personal reward fraction, ρ	0.7
Distribution parameters α, β	0, 1
Huber Loss parameter, δ	1
Number of episodes during training, B	1000
MellowMax parameter, ω	0.02, if $i \leq N/2$, 0.2, otherwise
Discount factor, γ	0.9
Optimizer	Adam
Optimizer learning rate	0.00025, if $i \leq N/2$, 0.0001, otherwise
Optimizer exponential decay rate for 1st, and 2nd moment estimates, β_1, β_2	0.9, 0.999
Optimizer epsilon for numerical stability, ϵ_{Adam}	10^{-7}
Global Replay Memory size, S_z	10^5
Number of decision points per network, T (also the size of the Local replay Memory)	20
NN architecture	
Number of hidden layer	3
Nodes at each layer	128
Number of skip connection (addition after activation)	2
Hidden layer activation function	Leaky-ReLU slop of 0.2
Output activation function	Identity
Weights initialization technique	Glorot-Uniform
Bias initialization	$\vec{0}$
Number of training steps, N_E	40
Batch size, b_z	32

TABLE II: A description of the hyper-parameter values used in the experiments conducted in this research.

facilitating communication and data exchange. In addition, using the masking approach not only depends on the presence or absence of a control channel for communication but also helps to fast convergence in case of higher action space, as shown in previous work [52]–[55]. When directing our attention to the physical results obtained during the training process, it is evident that CARLTON exhibits noteworthy enhancements in the mean, median, and minimum values of the channel quality. The improvement of these values, as defined in (18), are shown in Figure 4. Furthermore, upon convergence, it is conspicuous that the agents have acquired the ability to cooperate effectively, resulting in a scenario where the lowest channel quality (min_{CQ}) of some agents in the system remains above 0.95 percent. Here, $c^n(t)$ is the channel of network n at time step t .

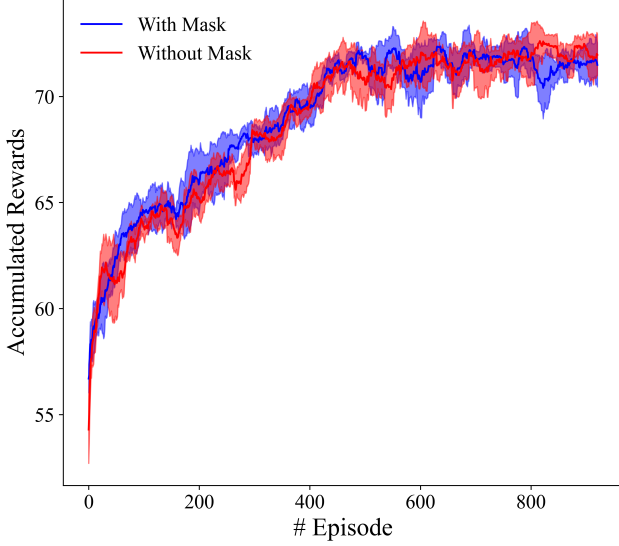


Fig. 3: CARLTON performance: The accumulated rewards as function of episode number during training for implementation of with and without masking approach. In a case of perfect game the maximum value is 88.

$$\begin{aligned}
 \text{CQ} &= \left[\text{QV}_{c^1(T)}^1(T), \dots, \text{QV}_{c^N(T)}^N(T) \right], \\
 \overline{\text{CQ}} &= \mathbb{E}[\text{CQ}], \\
 \widetilde{\text{CQ}} &= \text{Median}(\text{CQ}), \\
 \min_{\text{CQ}} &= \min(\text{CQ}).
 \end{aligned} \tag{18}$$

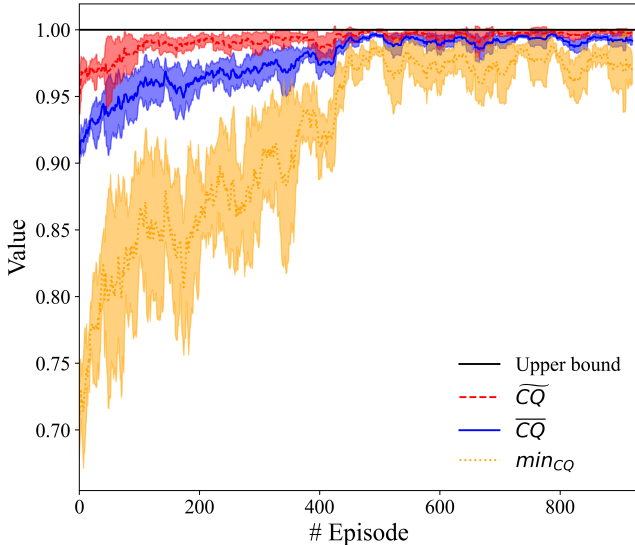


Fig. 4: CARLTON performance: The empirical results of the mean ($\overline{\text{CQ}}$), median ($\widetilde{\text{CQ}}$), minimum (\min_{CQ}) values of channel quality during training.

Similarly, we have investigated the progress observed during training regarding supplementary physical parameters. The first additional parameter is the average number of channel changes (ANCC), defined as the average number of channel

changes until convergence per network. The ANCC score (ANCCS) is given by:

$$\text{ANCCS} = 1 - \frac{\text{ANCC}}{T}. \tag{19}$$

The second parameter is the convergence time (CT), which refers to the time of the last channel change made by one of the networks during the scenario. The convergence time score (CTS) is calculated as follows:

$$\text{CTS} = 1 - \frac{\text{CT}}{T \cdot N}. \tag{20}$$

The third parameter, denoted as spectrum efficiency (SE), is intended to assess the spectral distortion resulting from the utilization of networks after convergence or at the end of the episode. A higher value of SE parameter indicates that the integration of a new network into the group becomes an easier task by providing more channels with high quality to operate on, along with causing minimal distortion to the convergences solution achieved by the earlier participants. The SE score (SES) is computed as follows:

$$\text{SES} = \mathbb{E}[\Psi] = \frac{1}{N} \sum_{n=1}^N \Psi^n,$$

where

$$\Psi^n = \left(\sum_{k=1}^K (\text{QV}_k^n(T))^2 \right)^{0.5} / K^{0.5}.$$

The last parameter that we define is a linear weighted score (WS) of the parameters of interest, given by:

$$\text{WS} = w_1 \cdot \overline{\text{CQ}} + w_2 \cdot \text{ANCCS} + w_3 \cdot \text{CTS} + w_4 \cdot \text{SES}, \tag{22}$$

where we set w_1, w_2, w_3, w_4 in the simulations to 0.4, 0.1, 0.4, 0.1, respectively.

As apparent from Figure 5, all parameter scores, except SE, demonstrate improvement. These results align with our reward function, as specified in (13), wherein the impact of the CT and ANCC on the reward value is given in line 10 in Algorithm 2. Moreover, in view of the absence of a direct motivation to enhance the SE score, the algorithm possesses the freedom to establish an SE score that harmonizes with the converged policy, and results in an average value of approximately 0.8 for the SE score.

Moreover, we conducted an analysis of the influence of the personal reward weight, denoted as ρ in (13), on the algorithm's physical behavior. All options were tested over 30 games for each scenario, where the scenarios differed by the number of networks participating, ranging from 2 to 15 networks. In total, this amounted to 420 games. Despite the training process being limited to scenarios involving a maximum of 7 networks, our examination extends to include the evaluation of the algorithm's generalization capabilities across scenarios with a larger number of participating networks. It was observed that, with respect to the metric WS as depicted in Figure 6, higher values demonstrated superior performance and enhanced generality. Conversely, in the context of CQ and \min_{CQ} , lower values exhibited better performance, as

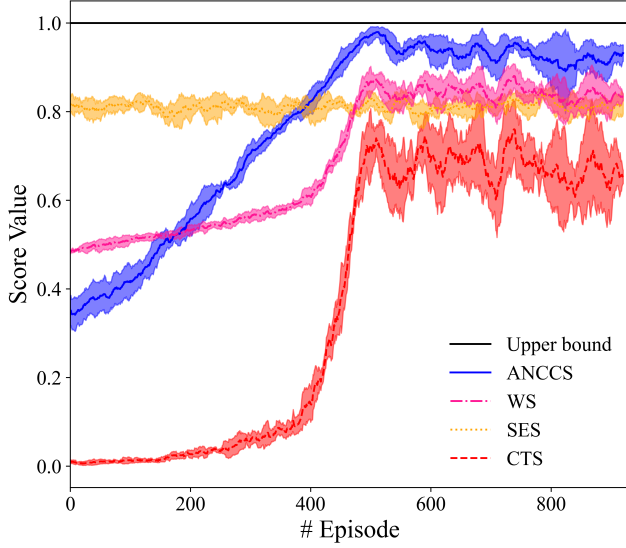


Fig. 5: CARLTON performance: The score values of the average number of channel changes (ANCC), convergence time (CT), spectrum efficiency (SE), and the weighted score (WS) during training.

evidenced by the expectation of the mean value displayed in Figure 7. This disparity in results can be attributed to the fact that higher values lead to more aggressive policies, resulting in quicker convergence. On the other hand, lower values facilitated increased cooperation and fairness among the participating networks, leading to a slower but more stable mechanism. A value of 0.7 was found to effectively strike a balance between these two contrasting aspects, rendering it an effective selection. In the context of cooperative missions, this equilibrium point is particularly noteworthy, as it arises from the operational constraints of decentralized agents without information exchange capabilities, effectively achieving equilibrium between self-interest and social responsibility.

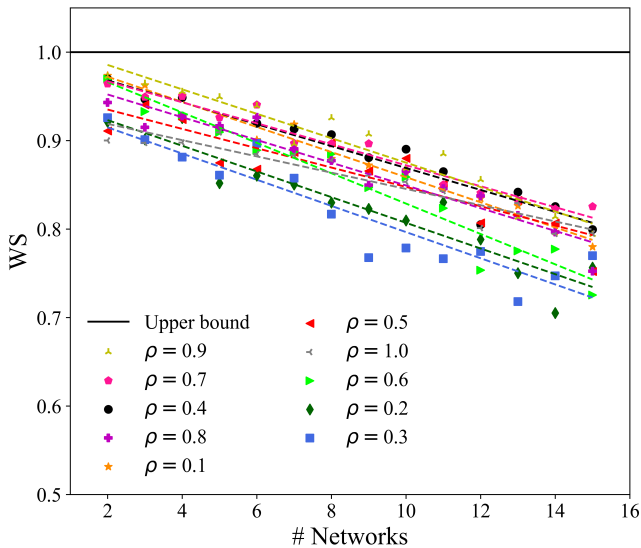


Fig. 6: CARLTON performance: The weighted score value, WS, as a function of the number of networks participating in the scenario for different values of ρ .

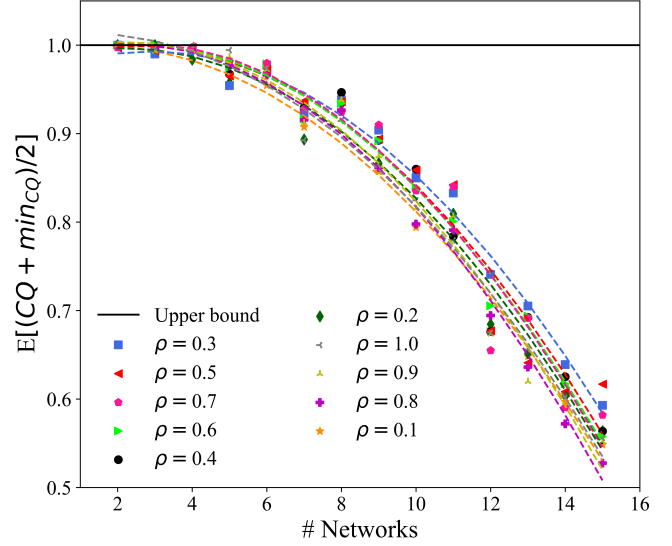


Fig. 7: CARLTON performance: the expectation of the mean value of CQ and \min_{CQ} as a function of the number of networks participating in the scenario for different values of ρ .

Afterward, we conducted an analysis pertaining to the influence of a designated threshold parameter denoted as Γ , which serves to establish the criteria for considering networks as neighbors. To briefly recapitulate, if the ED between the central points of two networks falls below the threshold Γ , both networks are deemed neighbors. These neighbor networks influence each other's rewards through the parameter denoted as r_{sw} , as shown in (13) and elaborated in Algorithm 3. In the scenario where Γ approaches zero ($\Gamma \rightarrow 0 [m]$), each network progressively exhibits more self-centered behavior, prioritizing its individual performance exclusively. Conversely, when Γ tends towards infinity ($\Gamma \rightarrow \infty$), each network gradually adopts a more socialistic stance, with its reward encompassing a broader spectrum of network performances, including those with which it shares no direct impact on their QVs. For example, when the Euclidean Distance (ED) between the central points equal to $700[m]$, there exists a 3% probability that the two networks will exert an influence on each other's QVs. Our analysis unveiled that, concerning WS performance, designating a network as a neighbor when the distance falls below 500 meters (corresponding to a probability of 50% that both networks influence each other's QVs) within the environmental framework described in Section II-B), yielded the highest average performance across all tested scenarios, as depicted in Figure 8.

On the contrary, when we shift our attention to the expectation value of $[(CQ + \min_{CQ})/2]$, it becomes evident that $\Gamma = 400$ meters (representing a probability of 86% that the networks impact each other's QVs) yields the most favorable average value across the entire domain under examination, as illustrated in Figure 9. These findings underscore the notion that, in order to achieve a high level of social performance encompassing all participants within the given scenario, a network should only consider interactions with those networks that have a high probability of interaction. This concept not

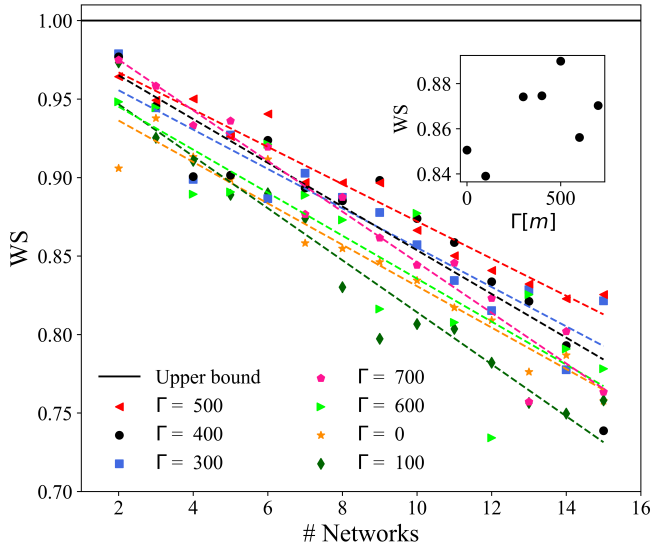


Fig. 8: CARLTON performance: The weighted score value, WS, as a function of the number of networks participating in the scenario for different values function of Γ [m]. Inset: The average value of WS across all scenarios as function of Γ [m].

only benefits individual performance but also augments the performance of the entire system. Conversely, it is evident that adopting and learning a selfish policy ($\Gamma = 0$) exhibits the least favorable performance across all scenarios examined. It is noteworthy that when taking into account the average of both parameters, $\Gamma = 500$ meters stands out as the leading choice.

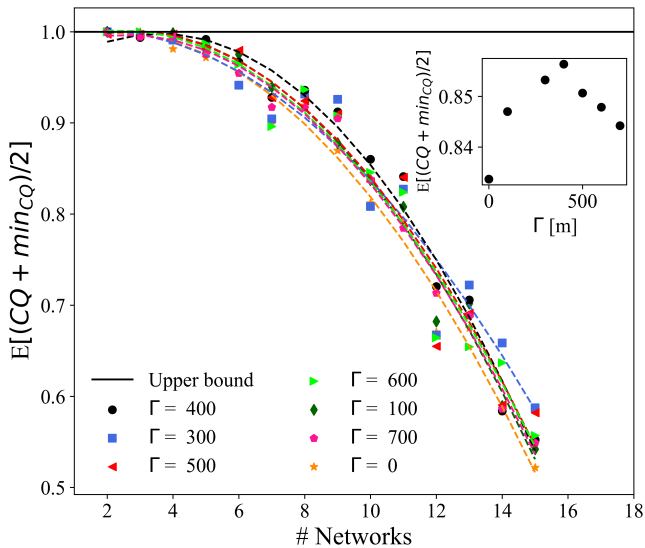


Fig. 9: CARLTON performance: The expectation of the mean value of CQ and \min_{CQ} as a function of the number of networks participating in the scenario for different values of Γ [m]. Inset: The average value of $E[(CQ + \min_{CQ})/2]$ across all scenarios as function of Γ [m].

Subsequently, we sought to further enhance the performance of our proposed algorithm by implementing a post-processing step in the decision-making mechanism. Given the algorithm's generalization across diverse and extensive domains involving

varying numbers of participating networks, certain instances of unnecessary channel switches were observed. For example, in a 2-network scenario, the algorithm would switch from a channel with a CQ of 1.0 to another channel with the same CQ value, even when this switching had no impact on the other participant. Such occurrences are a result of the algorithm's generalization mechanism, which has learned to create sparsity and adopt policies that aim to provide favorable performance in numerous situations. To address this issue, we introduced a post-processing step as follows: If the CQ of the desired channel is not greater than the CQ of the current channel by at least $\varphi\%$, the algorithm maintains its current channel, and effectively abstained from unnecessary changes. However, if the difference in CQ values exceeds the specified threshold, the algorithm follows the proposed action and executes the channel switch accordingly. The baseline algorithm, without post-processing, is denoted by $\varphi = \text{None}$. Furthermore, in multi-agent systems with a high number of members, it can be challenging to account for every possible scenario. Consequently, the agents tend to learn policies that exhibit bias toward the scenarios within the training set. Applying a threshold based on channel quality can reduce unnecessary spectrum mobility, which serves as a post-processing block. To illustrate, consider a scenario in which a single network, initially operating on a randomly selected channel, might transition to an alternative channel without any rational reason, a behavior likely stemming from the biased policy learned by the agents.

The findings illustrate a correlation between the increase in the weighted score as the threshold value, φ , increases, as evident from the observations in Figure 10. Conversely, there is a decrease in the channel quality, as represented in Figure 11. This indicates that the inclusion of the threshold significantly expedites the convergence time, albeit at the cost of achieving a better solution concerning channel quality. The selection of the optimal threshold value is contingent upon two crucial factors, the size of the network, where the switch to another channel can be expensive in terms of communication operations, and the quality threshold set by the user. These considerations emphasize the significance of setting a thoughtful threshold to achieve a trade-off between convergence speed and channel quality. The introduction of a post-decision mechanism, as an optional modification, holds promise for overall performance enhancement, thereby warranting further investigation and experimentation to assess its potential benefits fully.

B. Performance Comparison

We now present a comprehensive comparative analysis to assess the performance of CARLTON compared to other well-known algorithms. To establish an upper bound, we considered an algorithm based on graph coloring, which operates in a centralized manner and is not suitable for distributed implementations. Furthermore, we conducted a comprehensive evaluation of CARLTON against alternative approaches, including Jammer Avoidance Response (JAR) [46]. In the case of JAR, designed to mitigate interference or jamming, the algorithm

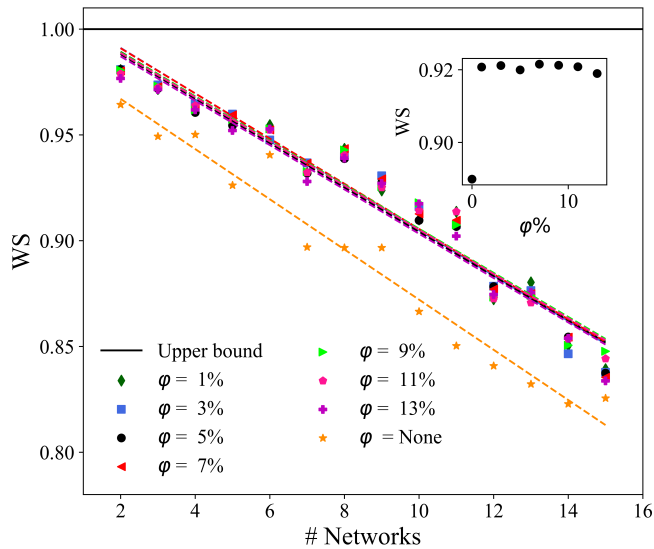


Fig. 10: CARLTON performance: The expectation of the weighted score, WS, as a function of participating network at each scenario. Inset: The average value of WS across all scenarios as function of the threshold value φ , 0 stands for None.

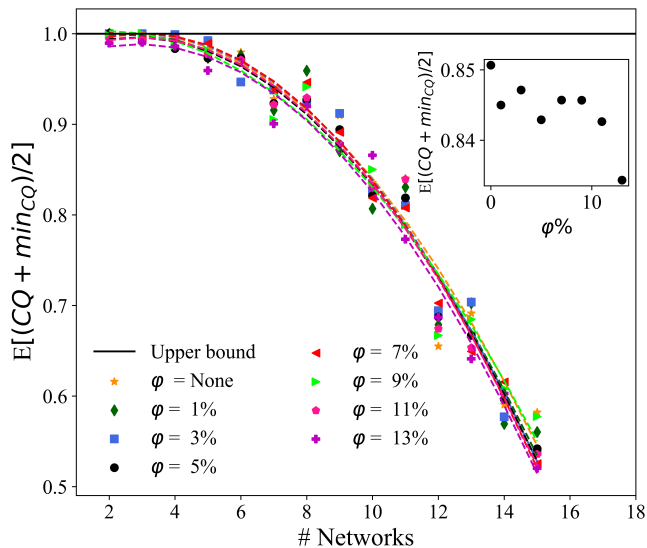


Fig. 11: CARLTON performance: The expectation of the average between CQ and \min_{CQ} as a function of participating network at each scenario. Inset: The average value of $E[(CQ + \min_{CQ})/2]$ across all scenarios as function of the threshold value φ , 0 stands for None.

draws inspiration from electric fish mobility, aiming to identify potential jamming and autonomously shift its electric discharge frequency away from the potential jamming frequency. JAR executes channel switches to nearby channels ($\pm 2MHz$) only if such switches can enhance the channel quality by a margin of at least 0.05. This approach has demonstrated state-of-the-art results within the considered model compared to existing methods. Additionally, we evaluated against the well-known Random Agent (RA) [20] static initialization, where we randomly set the initial channel and refrain from making any further channel switches. The comparison with these alternative algorithms provided valuable insights into

the effectiveness and advantages of CARLTON within the considered model.

In a manner analogous to the comparison involving ρ , all algorithms underwent testing across the identical set of 420 games. The obtained results demonstrated the superior performance of CARLTON in terms of both the WS metric and the expectation of $[CQ + \min_{CQ}]/2$ values, as illustrated in Figure 12 and Figure 13, respectively.

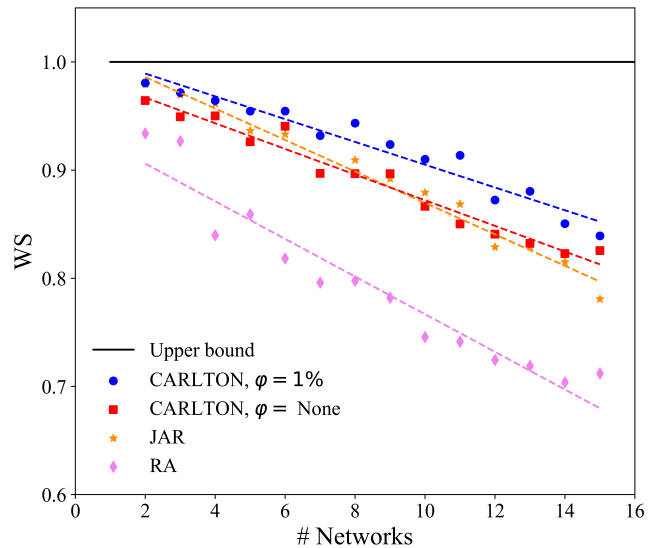


Fig. 12: Algorithm comparison: The weighted score value, WS, as a function of the number of networks participating in the scenario.

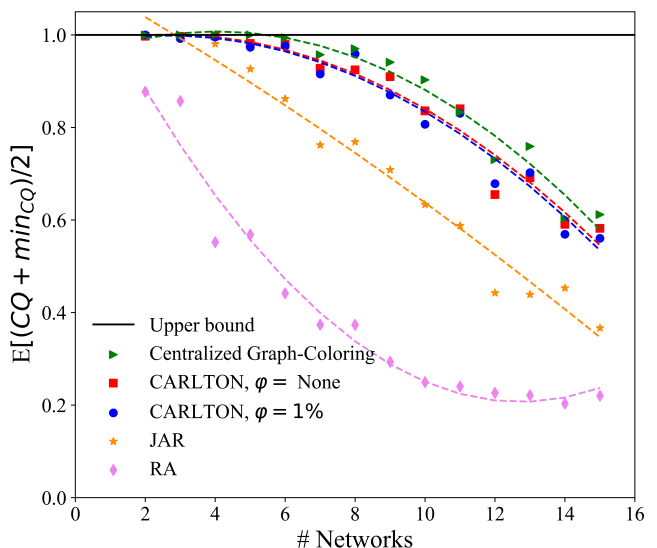


Fig. 13: Algorithm comparison: The expectation of the mean value of CQ and \min_{CQ} as a function of the number of networks participating in the scenario.

Nevertheless, as shown in Figure 14, the convergence time score demonstrates lower values in the case of CARLTON without post-processing ($\varphi = \text{None}$), indicating that achieving superior performance in channel quality required a more

comprehensive interaction among the network participants than alternative algorithms, translating into a longer time. Furthermore, CARLTON displayed a marginal difference of only 2% compared to the centralized graph-coloring approach in the in-sample domain (i.e., $\#Networks < 7$), underscoring its efficacy in distributed systems, as illustrated in Figure 15.

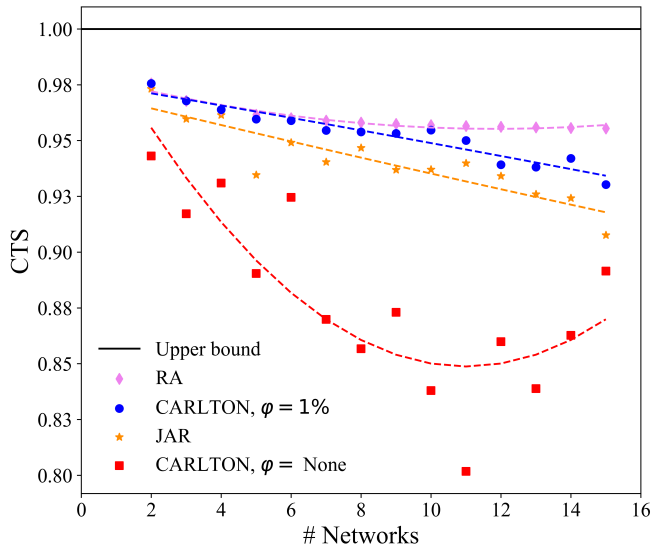


Fig. 14: Algorithm comparison: The convergence time score (CTS) as a function of the number of networks participating in the scenario.

Finally, the obtained results unequivocally demonstrate the exceptional performance of CARLTON, even in scenarios where it was not explicitly trained on (i.e., $\#Networks > 7$, named out-of-sample), thereby highlighting its remarkable generality. This remarkable adaptability can be attributed to the underlying concept that scenarios with a high number of networks in certain constellations can be effectively represented by combinations of multiple scenarios involving a lower number of networks. Consequently, the agent exhibits cooperation not with all networks but rather selectively with a subset, likely comprising fewer than 7 networks, which are considered its neighboring networks. This premise elucidates the compelling rationale behind the observed excellent generality.

V. CONCLUSION

We have introduced a novel distributed DCA algorithm, dubbed CARLTON, designed for multi-agent systems within the framework of MARL. CARLTON is specifically tailored for scenarios involving non-orthogonal operating channels with ICI, necessitating cooperation among participating networks to enhance spectral efficiency. The key emphasis of CARLTON lies in networks with a substantial number of users, aiming to achieve both high channel quality and rapid convergence. Our experimental results highlight the superior performance of CARLTON compared to alternative approaches, exhibiting only a marginal trade-off in channel quality when compared to the centralized-based graph-coloring approach.

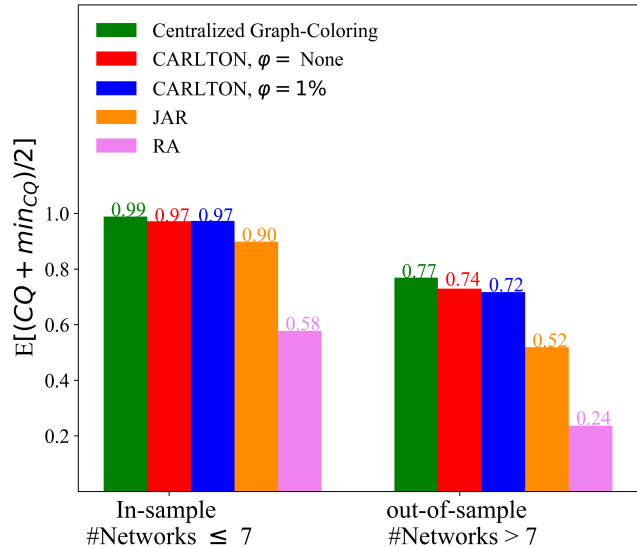


Fig. 15: Algorithm comparison: The average value of $E[(CQ + \min_{CQ})/2]$ across all scenarios for each algorithm. For CARLTON $\phi = 0$.

Moreover, CARLTON demonstrates remarkable generalization capabilities, effectively handling scenarios that were not encountered during training (out-of-sample scenarios). This effectiveness positions CARLTON as an exceptional algorithm for proficiently managing DCA among distributed cognitive networks in complex interference environments.

REFERENCES

- [1] K. Liu and Q. Zhao, "Cooperative game in dynamic spectrum access with unknown model and imperfect sensing," *IEEE Transactions on Wireless Communications*, vol. 11, no. 4, pp. 1596–1604, 2012.
- [2] C. Tekin and M. Liu, "Online learning of rested and restless bandits," *IEEE Transactions on Information Theory*, vol. 58, no. 8, pp. 5588–5611, 2012.
- [3] H. Liu, K. Liu, and Q. Zhao, "Learning in a changing world: Restless multiarmed bandit with unknown dynamics," *IEEE Transactions on Information Theory*, vol. 59, no. 3, pp. 1902–1916, 2013.
- [4] N. Nayyar, D. Kalathil, and R. Jain, "On regret-optimal learning in decentralized multiplayer multiarmed bandits," *IEEE Transactions on Control of Network Systems*, vol. 5, no. 1, pp. 597–606, 2016.
- [5] O. Avner and S. Mannor, "Multi-user lax communications: a multi-armed bandit approach," in *IEEE INFOCOM 2016-The 35th Annual IEEE International Conference on Computer Communications*, pp. 1–9, IEEE, 2016.
- [6] I. Bistriz and A. Leshem, "Distributed multi-player bandits—a game of thrones approach," in *Advances in Neural Information Processing Systems*, pp. 7222–7232, 2018.
- [7] T. Gafni and K. Cohen, "Learning in restless multi-armed bandits via adaptive arm sequencing rules," *IEEE Transactions on Automatic Control*, 2020.
- [8] W. Wang, A. Leshem, D. Niyato, and Z. Han, "Decentralized learning for channel allocation in iot networks over unlicensed bandwidth as a contextual multi-player multi-armed bandit game," *IEEE Transactions on Wireless Communications*, vol. 21, no. 5, pp. 3162–3178, 2021.
- [9] T. Gafni, M. Yemini, and K. Cohen, "Learning in restless bandits under exogenous global markov process," *IEEE Transactions on Signal Processing*, vol. 70, pp. 5679–5693, 2022.
- [10] A. Leshem, E. Zehavi, and Y. Yaffe, "Multichannel opportunistic carrier sensing for stable channel access control in cognitive radio systems," *IEEE Journal on Selected Areas in Communications*, vol. 30, no. 1, pp. 82–95, 2012.
- [11] T. Gafni and K. Cohen, "Distributed learning over markovian fading channels for stable spectrum access," *IEEE Access*, vol. 10, pp. 46652–46669, 2022.

- [12] Z. Han, Z. Ji, and K. R. Liu, "Fair multiuser channel allocation for OFDMA networks using Nash bargaining solutions and coalitions," *IEEE Transactions on Communications*, vol. 53, no. 8, pp. 1366–1376, 2005.
- [13] I. Menache and N. Shimkin, "Rate-based equilibria in collision channels with fading," *IEEE Journal on Selected Areas in Communications*, vol. 26, no. 7, pp. 1070–1077, 2008.
- [14] I. Menache and A. Ozdaglar, "Network games: Theory, models, and dynamics," *Synthesis Lectures on Communication Networks*, vol. 4, no. 1, pp. 1–159, 2011.
- [15] L. M. Law, J. Huang, and M. Liu, "Price of anarchy for congestion games in cognitive radio networks," *IEEE Transactions on Wireless Communications*, vol. 11, no. 10, pp. 3778–3787, 2012.
- [16] K. Cohen, A. Leshem, and E. Zehavi, "Game theoretic aspects of the multi-channel ALOHA protocol in cognitive radio networks," *IEEE Journal on Selected Areas in Communications*, vol. 31, pp. 2276–2288, 2013.
- [17] H. Wu, C. Zhu, R. J. La, X. Liu, and Y. Zhang, "Fasa: Accelerated S-ALOHA using access history for event-driven M2M communications," *IEEE/ACM Transactions on Networking (TON)*, vol. 21, no. 6, pp. 1904–1917, 2013.
- [18] C. Singh, A. Kumar, and R. Sundaresan, "Combined base station association and power control in multichannel cellular networks," *IEEE/ACM Transactions on Networking*, vol. 24, no. 2, pp. 1065–1080, 2016.
- [19] K. Cohen and A. Leshem, "Distributed game-theoretic optimization and management of multichannel aloha networks," *IEEE/ACM Transactions on Networking*, vol. 24, no. 3, pp. 1718–1731, 2016.
- [20] K. Cohen, A. Nedić, and R. Srikant, "Distributed learning algorithms for spectrum sharing in spatial random access wireless networks," *IEEE Transactions on Automatic Control*, vol. 62, no. 6, pp. 2854–2869, 2017.
- [21] D. Malachi and K. Cohen, "Queue and channel-based aloha algorithm in multichannel wireless networks," *IEEE Wireless Communications Letters*, vol. 9, no. 8, pp. 1309–1313, 2020.
- [22] O. Naparstek and K. Cohen, "Deep multi-user reinforcement learning for dynamic spectrum access in multichannel wireless networks," in *GLOBECOM 2017-2017 IEEE Global Communications Conference*, pp. 1–7, IEEE, 2017.
- [23] O. Naparstek and K. Cohen, "Deep multi-user reinforcement learning for distributed dynamic spectrum access," *IEEE transactions on wireless communications*, vol. 18, no. 1, pp. 310–323, 2018.
- [24] H.-H. Chang, H. Song, Y. Yi, J. Zhang, H. He, and L. Liu, "Distributive dynamic spectrum access through deep reinforcement learning: A reservoir computing-based approach," *IEEE Internet of Things Journal*, vol. 6, no. 2, pp. 1938–1948, 2018.
- [25] P. Yang, L. Li, J. Yin, H. Zhang, W. Liang, W. Chen, and Z. Han, "Dynamic spectrum access in cognitive radio networks using deep reinforcement learning and evolutionary game," in *2018 IEEE/CIC International Conference on Communications in China (ICCC)*, pp. 405–409, IEEE, 2018.
- [26] W. Su, J. Lin, K. Chen, L. Xiao, and C. En, "Reinforcement learning-based adaptive modulation and coding for efficient underwater communications," *IEEE access*, vol. 7, pp. 67539–67550, 2019.
- [27] Y. Zhang, X. Wang, and Y. Xu, "Energy-efficient resource allocation in uplink noma systems with deep reinforcement learning," in *2019 11th international conference on wireless communications and signal processing (WCSP)*, pp. 1–6, IEEE, 2019.
- [28] D. Lee, Y. G. Sun, S. H. Kim, I. Sim, Y. M. Hwang, Y. Shin, D. I. Kim, and J. Y. Kim, "Dqn-based adaptive modulation scheme over wireless communication channels," *IEEE Communications Letters*, vol. 24, no. 6, pp. 1289–1293, 2020.
- [29] W. Ning, X. Huang, K. Yang, F. Wu, and S. Leng, "Reinforcement learning enabled cooperative spectrum sensing in cognitive radio networks," *Journal of Communications and Networks*, vol. 22, no. 1, pp. 12–22, 2020.
- [30] J. Xu, H. Lou, W. Zhang, and G. Sang, "An intelligent anti-jamming scheme for cognitive radio based on deep reinforcement learning," *IEEE Access*, vol. 8, pp. 202563–202572, 2020.
- [31] F. Obite, A. D. Usman, and E. Okafor, "An overview of deep reinforcement learning for spectrum sensing in cognitive radio networks," *Digital Signal Processing*, vol. 113, p. 103014, 2021.
- [32] X. Du, T. Wang, Q. Feng, C. Ye, T. Tao, L. Wang, Y. Shi, and M. Chen, "Multi-agent reinforcement learning for dynamic resource management in 6g in-x subnetworks," *IEEE Transactions on Wireless Communications*, vol. 22, no. 3, pp. 1900–1914, 2022.
- [33] R. Adeogun and G. Berardinelli, "Multi-agent dynamic resource allocation in 6g in-x subnetworks with limited sensing information," *Sensors*, vol. 22, no. 13, p. 5062, 2022.
- [34] Y. Bokobza, R. Dabora, and K. Cohen, "Deep reinforcement learning for simultaneous sensing and channel access in cognitive networks," *IEEE Transactions on Wireless Communications*, 2023.
- [35] R. Adeogun and G. Berardinelli, "Distributed channel allocation for mobile 6g subnetworks via multi-agent deep q-learning," in *2023 IEEE Wireless Communications and Networking Conference (WCNC)*, pp. 1–6, IEEE, 2023.
- [36] R. Paul, K. Cohen, and G. Kedar, "Multi-flow transmission in wireless interference networks: A convergent graph learning approach," *IEEE Transactions on Wireless Communications*, pp. 1–1, 2023.
- [37] S. Wang, H. Liu, P. H. Gomes, and B. Krishnamachari, "Deep reinforcement learning for dynamic multichannel access in wireless networks," *IEEE Transactions on Cognitive Communications and Networking*, vol. 4, no. 2, pp. 257–265, 2018.
- [38] V. Mnih, K. Kavukcuoglu, D. Silver, A. Graves, I. Antonoglou, D. Wierstra, and M. Riedmiller, "Playing atari with deep reinforcement learning," *arXiv preprint arXiv:1312.5602*, 2013.
- [39] M. Hessel, J. Modayil, H. Van Hasselt, T. Schaul, G. Ostrovski, W. Dabney, D. Horgan, B. Piot, M. Azar, and D. Silver, "Rainbow: Combining improvements in deep reinforcement learning," in *Proceedings of the AAAI conference on artificial intelligence*, vol. 32, 2018.
- [40] J. Schrittwieser, I. Antonoglou, T. Hubert, K. Simonyan, L. Sifre, S. Schmitt, A. Guez, E. Lockhart, D. Hassabis, T. Graepel, *et al.*, "Mastering atari, go, chess and shogi by planning with a learned model," *Nature*, vol. 588, no. 7839, pp. 604–609, 2020.
- [41] O. Vinyals, I. Babuschkin, W. M. Czarnecki, M. Mathieu, A. Dudzik, J. Chung, D. H. Choi, R. Powell, T. Ewalds, P. Georgiev, *et al.*, "Grandmaster level in starcraft ii using multi-agent reinforcement learning," *Nature*, vol. 575, no. 7782, pp. 350–354, 2019.
- [42] Y. Li, "Deep reinforcement learning: An overview," *arXiv preprint arXiv:1701.07274*, 2017.
- [43] Y. Xing, R. Chandramouli, S. Mangold, and N. SS, "Dynamic spectrum access in open spectrum wireless networks," *IEEE journal on selected areas in communications*, vol. 24, no. 3, pp. 626–637, 2006.
- [44] H. Van Hasselt, A. Guez, and D. Silver, "Deep reinforcement learning with double q-learning," in *Proceedings of the AAAI conference on artificial intelligence*, vol. 30, 2016.
- [45] S. Kim, K. Asadi, M. Littman, and G. Konidaris, "Deepmellow: removing the need for a target network in deep q-learning," in *Proceedings of the twenty eighth international joint conference on artificial intelligence*, 2019.
- [46] C. Huang, V. J. Sorger, M. Miscuglio, M. Al-Qadasi, A. Mukherjee, L. Lampe, M. Nichols, A. N. Tait, T. Ferreira de Lima, B. A. Marquez, *et al.*, "Prospects and applications of photonic neural networks," *Advances in Physics: X*, vol. 7, no. 1, p. 1981155, 2022.
- [47] J. J. Egly, "Radio propagation above 40 mc over irregular terrain," *Proceedings of the IRE*, vol. 45, no. 10, pp. 1383–1391, 1957.
- [48] A. Goldsmith, *Wireless communications*. Cambridge university press, 2005.
- [49] P. Auer, N. Cesa-Bianchi, Y. Freund, and R. E. Schapire, "The non-stochastic multiarmed bandit problem," *SIAM journal on computing*, vol. 32, no. 1, pp. 48–77, 2002.
- [50] K. Asadi and M. L. Littman, "An alternative softmax operator for reinforcement learning," in *International Conference on Machine Learning*, pp. 243–252, PMLR, 2017.
- [51] X. Glorot and Y. Bengio, "Understanding the difficulty of training deep feedforward neural networks," in *Proceedings of the thirteenth international conference on artificial intelligence and statistics*, pp. 249–256, JMLR Workshop and Conference Proceedings, 2010.
- [52] O. Vinyals, T. Ewalds, S. Bartunov, P. Georgiev, A. S. Vezhnevets, M. Yeo, A. Makhzani, H. Küttler, J. Agapiou, J. Schrittwieser, *et al.*, "Starcraft ii: A new challenge for reinforcement learning," *arXiv preprint arXiv:1708.04782*, 2017.
- [53] C. Berner, G. Brockman, B. Chan, V. Cheung, P. Debiak, C. Dennison, D. Farhi, Q. Fischer, S. Hashme, C. Hesse, *et al.*, "Dota 2 with large scale deep reinforcement learning," *arXiv preprint arXiv:1912.06680*, 2019.
- [54] D. Ye, Z. Liu, M. Sun, B. Shi, P. Zhao, H. Wu, H. Yu, S. Yang, X. Wu, Q. Guo, *et al.*, "Mastering complex control in moba games with deep reinforcement learning," in *Proceedings of the AAAI Conference on Artificial Intelligence*, vol. 34, pp. 6672–6679, 2020.
- [55] Y. Hou, X. Liang, J. Zhang, Q. Yang, A. Yang, and N. Wang, "Exploring the use of invalid action masking in reinforcement learning: A comparative study of on-policy and off-policy algorithms in real-time strategy games," *Applied Sciences*, vol. 13, no. 14, p. 8283, 2023.